Interstitial oxide ion conduction in (Sm2 − XZr x)Zr2O7 + δ

ARTICLE *in* SOLID STATE IONICS · SEPTEMBER 2014

Impact Factor: 2.56 · DOI: 10.1016/j.ssi.2014.01.028

6 AUTHORS, INCLUDING:

A.V. Shlyakhtina
Semenov Institute of Chemical Physics
60 PUBLICATIONS **478** CITATIONS
SEE PROFILE

D. A. Belov
Lomonosov Moscow State University
37 PUBLICATIONS **146** CITATIONS
SEE PROFILE

A. N. Streletskii
Semenov Institute of Chemical Physics
68 PUBLICATIONS **417** CITATIONS
SEE PROFILE

Solid State Ionics xxx (2014) xxx–xxx

Contents lists available at ScienceDirect

Solid State Ionics

journal homepage: www.elsevier.com/locate/ssi

Interstitial oxide ion conduction in $(Sm_{2-x}Zr_x)Zr_2O_{7+\delta}$

A.V. Shlyakhtina [a,*], D.A. Belov [a,b], A.V. Knotko [b], I.V. Kolbanev [a], A.N. Streletskii [a], L.G. Shcherbakova [a]

[a] Semenov Institute of Chemical Physics, Russian Academy of Sciences, ul, Kosygina 4, Moscow 119991, Russia
[b] Faculty of Chemistry, Moscow State University, Leninskie Gory 1, Moscow 119991, Russia

ARTICLE INFO

Article history:
Received 13 May 2013
Received in revised form 21 December 2013
Accepted 5 January 2014
Available online xxxx

Keywords:
Rare-earth zirconates
Oxygen interstitials
Oxygen vacancy
Fluorite
Pyrochlore

ABSTRACT

The crystal structure and transport properties of $(Sm_{2-x}Zr_x)Zr_2O_{7+x/2}$ (x = 0; 0.2; 0.32; 0.39; 0.48; 0.67; 0.78; 0.96; 1.14; 1.27) solid solutions have been investigated by X-ray techniques and impedance spectroscopy, respectively. The excess oxygen content of the composition with x = 0.2 has been determined by thermal analysis and mass spectrometry in a reducing atmosphere. The SmZrO system includes a two-phase (fluorite + pyrochlore) region for the $(Sm_{2-x}Zr_x)Zr_2O_{7+x/2}$ ($0.48 \le x < 0.96$) solid solutions. The interstitial oxide ion conductivity of the $(Sm_{2-x}Zr_x)Zr_2O_{7+x/2}$ ($0.2 \le x < 0.48$), 3×10^{-3} S/cm at 750 °C, is comparable to the vacancy-mediated conductivity of undoped $Sm_2Zr_2O_7$. The bulk conductivity of the interstitial oxide ion conductors $(Sm_{2-x}Zr_x)Zr_2O_{7+x/2}$ ($0.2 \le x < 0.48$) was shown to vary little in a wide range of Sm_2O_3 concentrations in contrast to the vacancy mediated oxide ion conductors $Sm_2(Zr_{2-x}Sm_x)O_{7-\delta}$ ($0 \le x < 0.29$).

1. Introduction

The Ln_2O_3–ZrO_2 (LnZrO; Ln = Sm, Gd) systems have been studied for a rather long time because they contain ZrO_2-based fluorite solid solutions (8–15 mol% Ln_2O_3 (Ln = Sm, Gd)), similar in oxide ion conductivity to the well-known solid electrolyte 92–85 mol% ZrO_2 with 8–15 mol% Y_2O_3, and the $Ln_2Zr_2O_7$ (Ln = Sm, Gd) compounds with the pyrochlore structure, which possess high oxide ion conductivity [1–6]. The ionic conductivity of pyrochlore $Sm_2Zr_2O_7$, first studied by Shinozaki et al. [1], is 3×10^{-3} S/cm at 800 °C. Above 814 °C, an electronic component emerges, and the type of conduction changes to ionic–electronic (mixed). Nominally stoichiometric $Ln_2Zr_2O_7$ zirconates of the intermediate lanthanides (Ln = Sm–Gd) actually contain cation antisite defects and oxygen vacancies and, strictly speaking, are always nonstoichiometric [7,8]. This feature of the intermediate rare-earth (RE) zirconates is attributable to the sufficiently small ionic radius mismatch between Ln^{3+} (Ln = Sm, Eu, Gd) ($R\,Ln^{3+}_{CN8}$ = 1.079, 1.066 and 1.053 Å) and Zr^{4+} ($R\,Zr^{4+}_{CN6}$ = 0.72 Å) [9]. Two types of $Sm_{2\pm x}Zr_{2\pm x}O_{7\pm\delta}$ solid solutions are possible [10], with oxide ion conductivity due to vacancies ($Sm_2(Zr_{2-x}Sm_x)O_{7-\delta}$) or interstitials ($(Sm_{2-x}Zr_x)Zr_2O_{7+\delta}$), as represented by the schemes:

$$(2\text{-}x)ZrO_2 + (1 + x/2)Sm_2O_3 \rightarrow (2\text{-}x)Zr_{Zr}^{\times} + xSm_{Zr}' + 2Sm_{Sm}^{\times} + (7\text{-}x/2)O_O^{\times} + x/2V_O^{\bullet\bullet}, \quad (1)$$

$$(2 + x)ZrO_2 + (1\text{-}x/2)Sm_2O_3 \rightarrow (2\text{-}x)Sm_{Sm}^{\times} + xZr_{Sm}^{\bullet} + 2Zr_{Zr}^{\times} + 7O_O^{\times} + x/2O_i''. \quad (2)$$

As shown for RE zirconate systems in [3,4,7,8,11–15], the highest oxide ion conductivity is offered by nominally stoichiometric $Ln_2Zr_2O_7$ (Ln = Sm, Eu, Gd, Tb) zirconates of the intermediate lanthanides (Ln = Sm–Gd), whereas the $Ln_2(Zr_{2-x}Ln_x)O_{7-\delta}$ (Ln = Sm–Gd, Tb; $0 < x \le 0.3$) substitutional solid solutions, with vacancy-mediated oxide ion conduction, have lower conductivity [2,3,16–19].

The extent of the $(Sm_{2-x}Zr_x)Zr_2O_{7+\delta}$ solid solutions, which lie in the ZrO_2–$Ln_2Zr_2O_7$ broad isomorphism range, is still the subject of controversy. In particular, according to Collongues [20] pyrochlore solid solutions exist in the ZrO_2–$Sm_2Zr_2O_7$ isomorphous miscibility range starting at 24 mol% Sm_2O_3, whereas Strickler and Carlson [4] reported solid solutions with this percentage of Sm_2O_3 to have the fluorite structure.

The main purpose of this work was to study the structure and transport properties of pyrochlore-like solid solutions in the composition range where oxide ion conduction by an interstitial mechanism is possible in $(Sm_{2-x}Zr_x)Zr_2O_{7+x/2}$ (x = 0.2 − 0.78). To ascertain whether an order–disorder (pyrochlore–defect fluorite) structural phase transition occurs in these systems, fluorite-like solid solutions containing 15, 12 and 10 mol% Sm_2O_3 (x = 0.96, 1.14, 1.27) were synthesized and their structural properties were investigated. In addition, we compared the interstitial oxide ion conductivity of $(Sm_{2-x}Zr_x)Zr_2O_{7+x/2}$ solid solutions with the vacancy-mediated conductivity of undoped $Sm_2Zr_2O_7$.

* Corresponding author. Tel.: +7 495 9397950; fax: +7 499 2420253.
E-mail addresses: annash@chph.ras.ru, annashl@inbox.ru (A.V. Shlyakhtina).

0167-2738/$ – see front matter © 2014 Elsevier B.V. All rights reserved.
http://dx.doi.org/10.1016/j.ssi.2014.01.028

Table 1
Composition and structure of SmZrO solid solutions.

mol% Sm_2O_3 in SmZrO	x in $(Sm_{2-x}Zr_x)Zr_2O_{7+x/2}$	Structure of $(Sm_{2-x}Zr_x)Zr_2O_{7+x/2}$ (x = 0–1.27)
33.3	0	Pyrochlore, Fd3m
29	0.2	
26.6	0.32	
25.3	0.39	
23.5	0.48	Fluorite, Fm3m + pyrochlore, Fd3m
20	0.67	
18	0.78	
15	0.96	Fluorite, Fm3m
12	1.14	
10	1.27	

2. Experimental

$(Sm_{2-x}Zr_x)Zr_2O_{7+x/2}$ (x = 0; 0.2; 0.32; 0.39; 0.48; 0.67; 0.78; 0.96; 1.14; 1.27) solid solutions (the respective Sm_2O_3 contents are 33.3, 29, 26.6, 25.3, 23.5, 20, 18, 15, 12, and 10 mol%) were synthesized by reacting appropriate mixtures of Sm_2O_3 and ZrO_2 after mechanical activation in a SPEX8000 ball mill. Table 1 lists the compositions of the solid solutions, represented in two ways. The Sm_2O_3 starting powders were annealed at 1000 °C for 2 h and then placed in a desiccator after cooling to 850 °C. After the milling, the mixtures were pressed at 914 MPa and then fired at 1600 °C for 4–10 h. The density of the resultant samples was determined by measuring their mass and dimensions and ranged from 85 to 92% of their X-ray density. All of the synthesized solid solutions were characterized by X-ray diffraction (XRD) on a DRON-3M (filtered CuK_α radiation, step scan mode with a step of 0.05°, angular range 2θ = 13–65°) and a Rigaku D/MAX 2500 diffractometer (rotating anode, CuK_α radiation, 2θ = 10–100°, Rietveld refinement).

The microstructure of the sintered ceramics was examined using scanning electron microscopy (JEOL JSM-6390LA).

TG characterization was carried out using a Netzsch STA 449C system in combination with an AEOLOS-32 mass spectrometer between 25 and 800 °C (10 °C/min) in flowing H_2/Ar–He (reducing atmosphere) or in helium containing a small addition of oxygen (neutral atmosphere).

For electrical measurements disk-shaped polycrystalline samples (diameter of 6–9 mm and thickness of 1–3 mm) were prepared. Contacts to the sample faces were made by firing ChemPur C3605 paste, containing colloidal platinum, at 950–1000 °C.

The conductivity of $(Sm_{2-x}Zr_x)Zr_2O_{7+x/2}$ (x = 0–0.78) was characterized by impedance spectroscopy in air. The measurements were made in the frequency range 10 mHz to 3 MHz at 13 fixed temperatures from 300 to 1000 °C and an applied sinusoidal voltage of 0.5 V peak, using a Novocontrol Beta-N impedance analyzer and a NorECs ProboStat ceramic cell fitted with platinum electrodes and a Pt/Pt–Rh thermocouple. In data processing, we used ZView software [21].

3. Results and discussion

3.1. Structure and microstructure of the $(Sm_{2-x}Zr_x)Zr_2O_{7+x/2}$ (x = 0; 0.2; 0.32; 0.39; 0.48; 0.67; 0.78; 0.96; 1.14; 1.27) solid solutions

Fig. 1 shows the XRD patterns of the $(Sm_{2-x}Zr_x)Zr_2O_{7+x/2}$ (x = 0; 0.2; 0.32; 0.39; 0.48; 0.67; 0.78; 0.96; 1.14; 1.27) solid solutions synthesized at 1600 °C (10 h). In the XRD patterns of the $(Sm_{2-x}Zr_x)Zr_2O_{7+x/2}$ (x = 0–0.32) solid solutions, the intensity of the pyrochlore superstructure peaks (111), (311), (331), and (511) gradually decreases with decreasing Sm_2O_3 concentration (Fig. 1, curves 1–3). In the XRD patterns of the $(Sm_{2-x}Zr_x)Zr_2O_{7+x/2}$ (x = 0.39–0.78) solid solutions, the intensity of the pyrochlore superstructure peaks (111), (311), (331), and (511) is actually the same (Fig. 1, curves 4–7). The solid solutions $(Sm_{2-x}Zr_x)Zr_2O_{7+x/2}$ (x = 0.96, 1.14 and 1.27) are typical fluorites (Fig. 1, curves 8–10). Fig. 2 plots the unit-cell parameter (determined from XRD data)

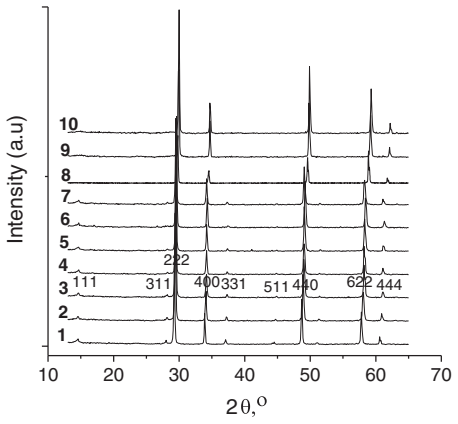

Fig. 1. XRD patterns of $(Sm_{2-x}Zr_x)Zr_2O_{7+x/2}$ (x = (1) 0; (2) 0.2; (3) 0.32; (4) 0.39; (5) 0.48; (6) 0.67; (7) 0.78; (8) 0.96; (9) 1.14; (10) 1.27) solid solutions prepared at 1600 °C (10 h).

against Sm_2O_3 concentration for the solid solutions obtained in the SmZrO system (a doubled lattice parameter is presented for the compositions with x = 0.96, 1.14 and 1.27). The composition dependence of the unit-cell parameter for the samarium system can be divided into 3 distinct portions (Fig. 2). Most likely, this system has a two-phase region (pyrochlore + fluorite solid solutions) in the $(Sm_{2-x}Zr_x)Zr_2O_{7+x/2}$ ($0.48 \le x < 0.96$) (Fig. 2, region II). In the two-phase region ($0.48 \le x < 0.96$) the data can be represented by a straight line. Similar data were obtained by Clements et al. [22] in studies of a fluorite–pyrochlore morphotropic phase transition in the $Ho_{2-y}Nd_yZr_2O_7$ solid-solution series. Neutron diffraction characterization showed that the solid solutions with y = 1–1.2 consisted of a mixture of fluorite and pyrochlore phases. According to the XRD data in Fig. 1 (scans 1–7), the XRD patterns of the $(Sm_{2-x}Zr_x)Zr_2O_{7+x/2}$ ($0 \le x \le 0.78$) solid solutions are consistent with the pyrochlore structure, i.e., they contain the main pyrochlore peaks. At the same time, the composition dependence of the unit-cell parameter in Fig. 2 strongly suggests that the $(Sm_{2-x}Zr_x)Zr_2O_{7+x/2}$ samples with $0.48 \le x < 0.96$ are two-phase. Since the pyrochlore and fluorite structures are closely related, the main fluorite peaks coincide with some of the pyrochlore peaks and cannot be differentiated in XRD patterns. The unit-cell parameters of eight pyrochlore-like $(Sm_{2-x}Zr_x)Zr_2O_{7+x/2}$ solid solutions with $0 \le x \le 0.78$ were determined more accurately using Rietveld refinement Fig. 3 shows Rietveld refinement profile for the $(Sm_{2-x}Zr_x)Zr_2O_{7+x/2}$ (x = 0.2). The assumption that all of the samples in this composition range were single-phase pyrochlores led to a slightly greater R_{wp} in the two-phase samples (x = 0.48, 0.67, 0.78) (Table 2). This is also evidence that the $(Sm_{2-x}Zr_x)Zr_2O_{7+x/2}$ system

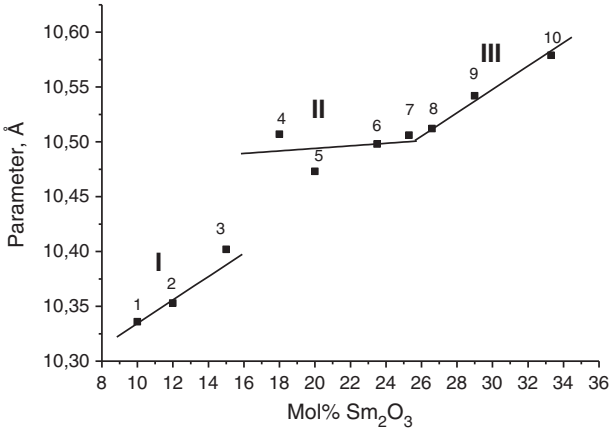

Fig. 2. Composition dependence of the unit-cell parameter for $(Sm_{2-x}Zr_x)Zr_2O_{7+x/2}$ (x = 0–1.27) solid solutions.

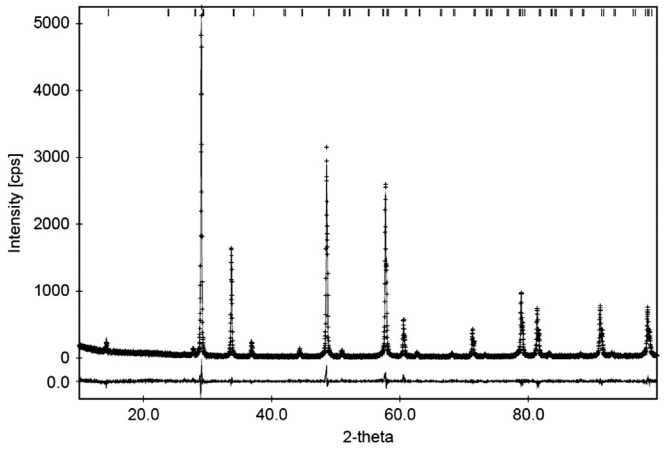

Fig. 3. Rietveld refinement profile for the materials containing $(Sm_{2-x}Zr_x)Zr_2O_{7+x/2}$ ($x = 0.2$).

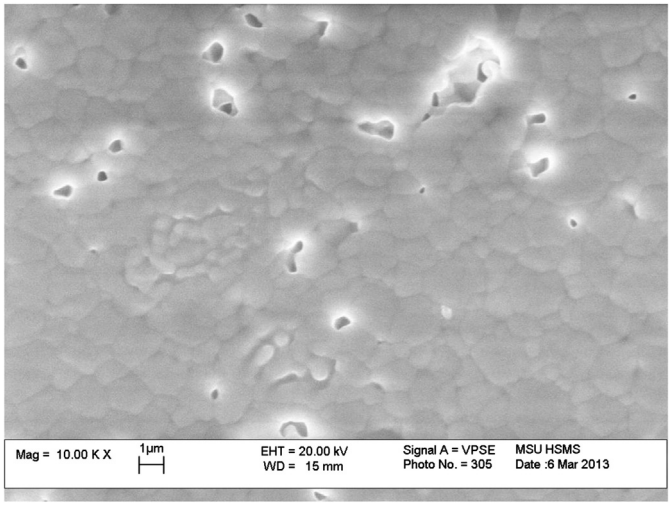

Fig. 4. SEM images of pyrochlore-like $(Sm_{2-x}Zr_x)Zr_2O_{7+x/2}$ ($x = 0.2$) solid solution.

has a two-phase region in the range $0.48 \le x < 0.96$. It can be seen from Table 2 that the fraction of antisite pairs in the $(Sm_{2-x}Zr_x)Zr_2O_{7+x/2}$ ($x = 0.2$–0.39) nonstoichiometric pyrochlore solid solutions increases from 3.5 to 5.9%. This is accompanied by an increase in the occupancy of interstitial oxygen in position 8b from 10.1 to 19.3%. The $(Sm_{2-x}Zr_x)Zr_2O_{7+x/2}$ ($x = 0.67$) solid solution contains 17.1% cation antisite defects according to Rietveld refinement (Table 2). This composition falls in the two-phase region and this result may be related to the co-existence of fluorite and pyrochlore phases in $(Sm_{2-x}Zr_x)Zr_2O_{7+x/2}$ ($x = 0.67$).

Thus, according to the present XRD data, the samarium system contains a two-phase region (pyrochlore + fluorite) in the composition range $0.48 \le x \le 0.78$. We should study the region of interstitial oxide ion conduction in $(Sm_{2-x}Zr_x)Zr_2O_{7+x/2}$ ($0.2 \le x < 0.48$).

Fig. 4 shows SEM image of thermally etched $(Sm_{2-x}Zr_x)Zr_2O_{7+x/2}$ ($x = 0.2$) sample. It is observed that the grain size of the pyrochlore-like solid solutions is a very weak function of their composition in the range $(Sm_{2-x}Zr_x)Zr_2O_{7+x/2}$ ($x = 0.2$–0.39) and ranges from 0.3 to 2 μm. Note that there are no second-phase inclusions, in accord with the XRD results.

3.2. Determination of excess oxygen in the $(Sm_{2-x}Zr_x)Zr_2O_{7+x/2}$ ($x = 0.2$; 0.32) solid solutions by reduction in the presence of hydrogen during TG measurements

Using the $(Sm_{2-x}Zr_x)Zr_2O_{7+x/2}$ ($x = 0.2$; 0.32) compositions as examples, we made the first attempt to estimate the excess oxygen content of the solid solutions from the weight loss during heating in the presence of hydrogen. Comparative experiments were performed in He and in the presence of hydrogen (H_2/Ar–He) in the cell of a DSC analyzer combined with a mass spectrometer. In both cases, the gas phase contained trace levels (~0.1%) of oxygen. Fig. 5a presents TG data for $(Sm_{2-x}Zr_x)Zr_2O_{7+x/2}$ ($x = 0.2$). The weight loss was 0.03% in He and 0.54% in the reducing atmosphere (H_2/Ar–He). The weight loss was accompanied by the formation of an appreciable amount of water, as was evidenced by an increase in ion current at $m/z = 18$ (Fig. 5). Thus, it is reasonable to conclude that the hydrogen reacted with the lattice oxygen to form water. The reaction occurred at temperatures from 180 to 1000 °C. Quantitative data have been obtained to date only for $(Sm_{2-x}Zr_x)Zr_2O_{7+x/2}$ ($x = 0.2$). The weight loss in this material was 0.54–0.03 = 0.51%, i.e. about twice the content of excess oxygen in this material (0.101 at.% = 0.28 wt.%) (Table 2).

We believe that the following processes take place in the interstitial oxide ion conductor $(Sm_{2-x}Zr_x)Zr_2O_{7+x/2}$ ($x = 0.2$) under reducing conditions:

1. Interstitial O^{2-} loses electrons, and the resulting neutral oxygen combines with hydrogen to form water:

$$O^{2-} - 2e' \rightarrow O$$

$$O + H_2 \rightarrow H_2O;$$

2. Samarium is a rare-earth cation that can be in two oxidation states (Sm^{2+} and Sm^{3+}). In the pyrochlore structure, samarium has a valence of 3+. Under reducing conditions, however, it can be reduced to Sm^{2+}:

$$Sm^{3+} + e' \rightarrow Sm^{2+}.$$

Thus, it is highly probable that, after reduction, pyrochlore-like $(Sm_{2-x}Zr_x)Zr_2O_{7+x/2}$ ($x = 0.2$) contains compounds of samarium in two oxidation states: Sm^{2+} and Sm^{3+}. Fig. 5b shows XRD patterns of $(Sm_{2-x}Zr_x)Zr_2O_{7+x/2}$ ($x = 0.2$) before heating (scan 1) and after thermal analysis in flowing He (scan 2) and in a H_2/Ar–He flow (scan 3). It is seen in Fig. 5b that, after reduction, $(Sm_{2-x}Zr_x)Zr_2O_{7+x/2}$ ($x = 0.2$) has extra lines at $2\theta = 30.3$; 51.3; and 59.2° (ZrO_2 marked by an

Table 2
XRD Rietveld refinement results for $(Sm_{2-x}Zr_x)Zr_2O_{7+x/2}$ ($0 \le x \le 0.78$).

mol% Sm_2O_3 in SmZrO	x in $(Sm_{2-x}Zr_x)Zr_2O_{7+x/2}$	$Zr_{Sm} + Sm_{Zr}$ antistructure pairs, %	Zr_{Sm}, antisite defects, %	Interstitial oxygen in position 8b	R_{wp}, %
33.3	0	8.1	–		5.3
29	0.2	3.5	10.1	0.10	12.96
26.6	0.32	5.9	16	0.16	12.68
25.3	0.39	5.2	19.3	0.19	12.88
23.5	0.48	6.9	23.9	0.24	15.2
20	0.67	17.1	33.5	0.34	15.34
18	0.78	6.2	39	0.39	16.77

Please cite this article as: A.V. Shlyakhtina, et al., Solid State Ionics (2014), http://dx.doi.org/10.1016/j.ssi.2014.01.028

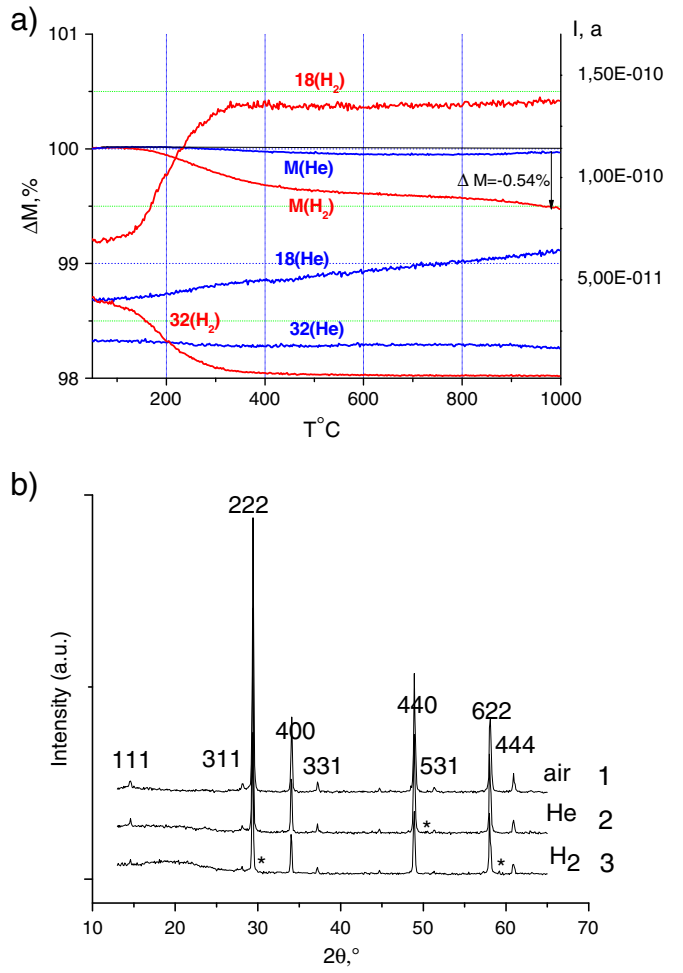

Fig. 5. (a) Variations in the sample weight, ion current for m/z = 18 (water) and ion current for m/z = 32 (oxygen) during heating of $(Sm_{2-x}Zr_x)Zr_2O_{7+x/2}$ (x = 0.2) in an inert atmosphere (He) and in the presence of hydrogen (H_2); (b) XRD patterns of $(Sm_{2-x}Zr_x)Zr_2O_{7+x/2}$ (x = 0.2) (1) in air, (2) after thermal analysis in He, and (3) after thermal analysis in a H_2 atmosphere.

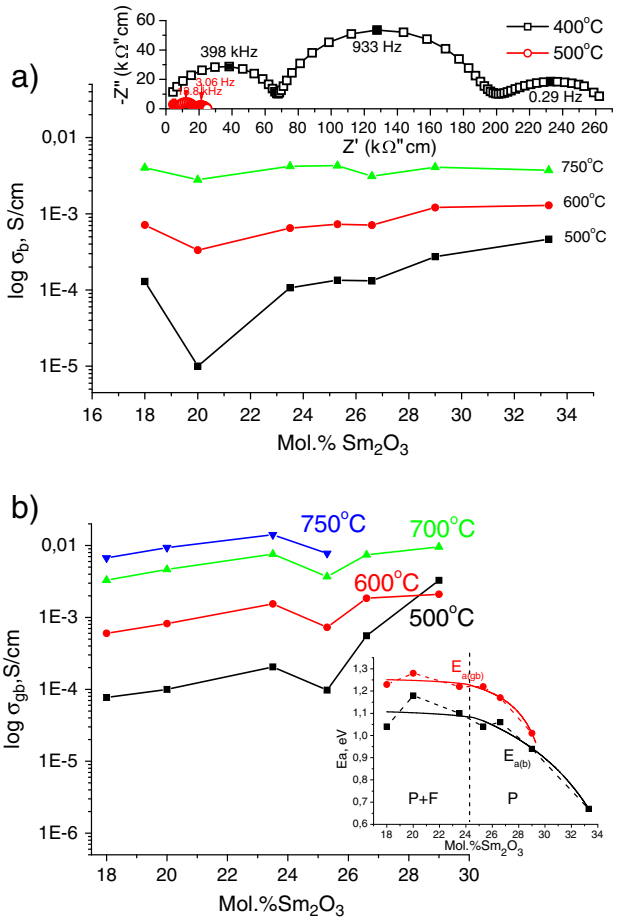

Fig. 6. Composition dependences of (a) bulk and (b) grain-boundary conductivity in $(Sm_{2-x}Zr_x)Zr_2O_{7+x/2}$ (x = 0–0.78) solid solutions, inset to a: impedance spectra of $(Sm_{2-x}Zr_x)Zr_2O_{7+x/2}$ (x = 0.39) at 400 and 500 °C and inset to b: composition dependences of the activation energies for bulk and grain-boundary conduction in $(Sm_{2-x}Zr_x)Zr_2O_{7+x/2}$ (x = 0–0.78) solid solutions.

asterisk) and the 311, 331, and 531 lines of the pyrochlore-like solid solution have reduced intensities. This suggests that a redox reaction occurred in the sample. Most likely, there is also a contribution from adsorbed oxygen and residual oxygen in the gas phase. It is because of the last factor that the total amount of oxygen evolved during the reduction exceeds that calculated with only the interstitial oxygen in the pyrochlore structure taken into account.

3.3. Transport properties of the $(Sm_{2-x}Zr_x)Zr_2O_{7+x/2}$ (x = 0; 0.2; 0.32; 0.39; 0.48; 0.67; 0.78) solid solutions

The impedance spectra of the solid solution $(Sm_{2-x}Zr_x)Zr_2O_{7+x/2}$ (x = 0.39) synthesized at 1600 °C are typical of traditional solid electrolytes and consist of three semicircles (Fig. 6a, inset). The impedance data can be described using the equivalent circuit proposed by Boukamp [23], which comprises three series connected elements, each composed of a parallel connected resistor and constant phase element (CPE, $Z_{CPE} = {}^{1}/_{C(i\omega)^p}$). The capacitance (C) values of the first, second, and third semicircles for $(Sm_{2-x}Zr_x)Zr_2O_{7+x/2}$ (x = 0.39) are given in Table 3 (for 500 °C) and clearly support their assignment to bulk, grain boundary and electrode contributions.

Fig. 6a and b presents the composition dependences of bulk and grain-boundary conductivities for all of the SmZrO pyrochlore-like samples annealed at 1600 °C for 10 h, except for the stoichiometric sample, which was fired for 4 h. After annealing at 1600 °C for 10 h, $Sm_2Zr_2O_7$ had low conductivity: 2×10^{-4} S/cm at 750 °C. The bulk conductivity of the SmZrO materials (Fig. 6a) varies little in the composition range $(Sm_{2-x}Zr_x)Zr_2O_{7+x/2}$ (x = 0.2–0.39) and is 3×10^{-3} S/cm at 750 °C. According to XRD data, the percentage of cation antistructure pairs increases in the $(Sm_{2-x}Zr_x)Zr_2O_{7+x/2}$ (x = 0.67) and the conductivity of this solid solution decreases slightly. As the Sm_2O_3 content decreases to 18 mol%, the bulk conductivity tends to increase. The most likely reason for this is the proximity of the region of fluorite-like solid electrolytes containing 8–12 mol% Sm_2O_3 and possessing high vacancy-mediated conductivity (~5×10^{-3} S/cm at 750 °C) [24]. It is worth noting that, at 20 mol% Sm_2O_3, lowering the measurement temperature from 750 to 500 °C increases the minimum in the composition dependence of bulk conductivity. This is typical of interfaces between regions differing in the predominant type of defect [25]. This confirms the presence of two types of solid solutions with vacancy-

Table 3
The 500 °C capacitance values and conductivities.

Composition	σ_{bulk}, $\times 10^{-4}$ S/cm	C_{bulk}, $\times 10^{-11}$ F	σ_{gb}^{app}, $\times 10^{-4}$ S/cm	C_{gb}, $\times 10^{-9}$ F	σ_{gb}^{sp}, $\times 10^{-6}$ S/cm	C_{el}, $\times 10^{-5}$ F
$(Sm_{2-x}Zr_x)Zr_2O_{7+x/2}$ (x = 0.67)	1.35	1.88	0.976	3.18	0.577	1.06

mediated and interstitial oxide ion conductivity in the SmZrO system (at low (≤12 mol%) and considerable (25.3–29 mol%) degrees of samarium oxide substitution for ZrO_2) in the ZrO_2–$Sm_2Zr_2O_7$ isomorphous miscibility range. The inset in Fig. 6b shows the composition dependences of the activation energies for bulk and grain-boundary conduction in the $(Sm_{2-x}Zr_x)Zr_2O_{7+x/2}$ (x = 0–0.78) pyrochlore-like solid solutions. The curves can also be divided into two portions. In the interstitial conduction region ($0.2 \le x < 0.48$), the activation energy increases rather steadily, whereas in the two-phase region ($0.48 \le x \le 0.78$) the data can be represented by a straight line.

4. Conclusions

Using XRD we have studied the structure of the $(Sm_{2-x}Zr_x)Zr_2O_{7+x/2}$ (x = 0–1.27) solid solutions, which lie in the ZrO_2–$Sm_2Zr_2O_7$ isomorphous miscibility range. All of the solid solutions in the composition range $(Sm_{2-x}Zr_x)Zr_2O_{7+x/2}$ ($0.2 \le x < 0.48$) have the disordered pyrochlore structure. The solid solutions at low degrees of samarium oxide substitution for ZrO_2 — $(Sm_{2-x}Zr_x)Zr_2O_{7+x/2}$ (x = 0.96; 1.14; 1.27) have a fluorite-like structure. According to XRD data, the SmZrO system contains a fluorite + pyrochlore two-phase region $(Sm_{2-x}Zr_x)Zr_2O_{7+x/2}$ ($0.48 \le x < 0.96$).

The excess oxygen content of the pyrochlore-like $(Sm_{2-x}Zr_x)Zr_2O_{7+x/2}$ (x = 0.2) solid solution has been determined by TG and mass spectrometry in flowing helium and a reducing atmosphere (H_2/Ar–He). The first to be released is the interstitial oxygen, and this process is initiated by the reduction of samarium ($Sm^{3+} + e' \rightarrow Sm^{2+}$) and accompanied by the formation of water. Most likely, there is also a contribution from adsorbed oxygen and residual oxygen in the gas phase. It is because of the last factor that the total amount of oxygen evolved during the reduction exceeds that calculated with only the interstitial oxygen in the pyrochlore structure taken into account.

The interstitial oxide ion conductivity of the $(Sm_{2-x}Zr_x)Zr_2O_{7+x/2}$ ($0.2 \le x < 0.48$) solid solutions, 3×10^{-3} S/cm at 750 °C, is comparable to the vacancy-mediated conductivity of undoped $Sm_2Zr_2O_7$. Note that, in studies of the region of vacancy-mediated oxide ion conduction in $Ln_2(Zr_{2-x}Ln_x)O_{7-\delta}$ (Ln = Sm, Gd; $0 \le x < 0.29$) pyrochlore solid solutions [3,19], their oxide ion conductivity was observed to drop sharply, whereas in studies of the region of interstitial oxide ion conduction in $(Sm_{2-x}Zr_x)Zr_2O_{7+x/2}$ ($0.2 \le x < 0.48$) materials their bulk conductivity was shown to vary little in a wide range of Sm_2O_3 concentrations.

Acknowledgments

This work was supported by the Russian Foundation for Basic Research (grant no. 13-03-00680) and the Chemistry and Materials Science Division of the Russian Academy of Sciences (basic research program no. 2: Advanced Metallic, Ceramic, Glassy, Polymeric, and Composite Materials).

References

[1] K. Shinozaki, M. Miyauchi, K. Kuroda, O. Sakurai, N. Mizutani, M. Kato, J. Am. Ceram. Soc. 62 (1979) 538.
[2] A.V. Shlyakhtina, I.V. Kolbanev, A.V. Knotko, M.V. Boguslavskii, S.Yu. Stefanovich, O.K. Karyagina, L.G. Shcherbakova, Inorg. Mater. 42 (2005) 975.
[3] A.V. Shlyakhtina, A.V. Knotko, M.V. Boguslavskii, S.Yu. Stefanovich, I.V. Kolbanev, L.L. Larina, L.G. Shcherbakova, Solid State Ionics 178 (2007) 59.
[4] D.W. Strickler, W.G. Carlson, J. Am. Ceram. Soc. 48 (1965) 286.
[5] J. Lefevre, M. Perez Y Jorba, R. Collongues, Bull. Soc. Chim. Fr. 12 (1959) 1969.
[6] T. Uehara, K. Koto, F. Kanamaru, Solid State Ionics 23 (1987) 137.
[7] R. Collongues, F. Queyroux, M. Perez Y Jorba, J.C. Jilles, Bull. Soc. Chim. Fr. 4 (1965) 1141.
[8] P.A. Arsent'ev, V.B. Glushkova, A.A. Evdokimov, E.K. Keler, V.B. Kravchenko, M.V. Kravchinskaya, V.A. Krzhizhanovskaya, A.K. Kuznetsov, Kh.M. Kurbanov, A.V. Potemkin, P.A. Tikhonov, M.N. Tseitlin, Rare-Earth Compounds: Zirconates, Hafnates, Niobates, Tantalates, and Antimonates, Moscow, Nauka, 1985.
[9] R.D. Shannon, C.T. Prewitt, Acta Crystallogr. B25 (1969) 925.
[10] M. Perez Y Jorba, Ann. Chem. 7 (1962) 479.
[11] Z.S. Volchenkova, Inorg. Mater. 5 (1969) 1096.
[12] M.P. van Dijk, F.C. Mijlhoff, A.J. Burgraaf, J. Solid State Chem. 62 (1986) 377.
[13] M.P. van Dijk, K.J. de Vries, A.J., Solid State Ionics 9 (1983) 913.
[14] M.P. van Dijk, A.N. Cormack, A.J. Burggraaf, C.R.A. Catlow, Solid State Ionics 17 (1985) 159.
[15] H. Yamamura, H. Nishino, K. Kakinuma, K. Nomura, Solid State Ionics 158 (2003) 359.
[16] T. van Dijk, K.J. de Vries, A.J. Byrggraaf, Phys. Status Solidi A 58 (1980) 115.
[17] A.V. Shlyakhtina, L.G. Shcherbakova, Russ. J. Electrochem. 1 (2012) 1.
[18] A.V. Shlyakhtina, L.G. Shcherbakova, Solid State Ionics 192 (2011) 200.
[19] T. Van Dijk, R.B. Helmholdt, A.J. Burggraaf, Phys. Status Solidi B 101 (1980) 765.
[20] R. Collongues, Ann. Chim. (Paris) 8 (1963) 395.
[21] ZView for Windows, Impedance/Gain Phase Analysis Software, Version 2.3f, Scribner Associates Inc., 2002.
[22] R. Clements, J.R. Hester, B.J. Kennedy, C.D. Ling, A.P.J. Atampfl, J. Solid State Chem. 184 (2011) 2108.
[23] B. Boukamp, Solid State Ionics 20 (1986) 31.
[24] W. Nernst, Z. Electrochem. 6 (1899) 41.
[25] Z.S. Volchenkova, D.S. Zubankova, Inorg. Mater. 23 (1987) 1175.

Please cite this article as: A.V. Shlyakhtina, et al., Solid State Ionics (2014), http://dx.doi.org/10.1016/j.ssi.2014.01.028